

BaCu₂Si₂O₇: a new quasi 1-dimensional $S = 1/2$ antiferromagnetic chain system

I. Tsukada, Y. Sasago,* and K. Uchinokura

Department of Applied Physics, The University of Tokyo, 7-3-1 Hongo, Bunkyo-ku, Tokyo 113-8656, Japan

A. Zheludev, S. Maslov, and G. Shirane

Physics Department, Brookhaven National Laboratory, Upton NY 11973-5000, USA

K. Kakurai

Neutron Scattering Laboratory, Institute for Solid State Physics, The University of Tokyo, Tokai, Ibaraki 319-1106, Japan

E. Ressouche

MDN/SPSMS/DRFMC CEN Grenoble, 17 rue des Martyrs, 38054 Grenoble Cedex, France

(April 26, 2024)

The new antiferromagnetic (AF) compound BaCu₂Si₂O₇ is studied by magnetic susceptibility and neutron scattering techniques. The observed behavior is dominated by the presence of loosely coupled $S = 1/2$ chains with the intrachain AF exchange constant $J_{\parallel} \approx 24.1$ meV. Long-range Néel ordering is observed below $T_N = 9.2$ K. The results are discussed within the framework of the Mean Field- RPA model for weakly interacting quantum spin chains.

I. INTRODUCTION

The amazing structural diversity of copper-oxide compounds makes these materials very useful as model systems for fundamental studies of low-dimensional magnetism. In most cases their unique properties result from the particular topologies of the corresponding spin networks formed by magnetic Cu²⁺ ions. Examples of such networks are found in CuGeO₃ (linear chain: spin-Peierls),¹ CaCuGe₂O₆ (isolated dimer),^{2,3} BaCuSi₂O₆ (two-dimensional bilayer),⁴ Sr₂CuO₃ (rigid linear chain),⁵ SrCu₂O₃ (two-leg ladder),⁶ and SrCuO₂ (edge-shared double linear chain),⁷ etc. Magnetic interactions in all these systems are determined by the microscopic spatial coordination of Cu²⁺ and O²⁻.⁸ The so-called corner-sharing (\angle Cu-O-Cu $\approx 180^\circ$) and edge-sharing (\angle Cu-O-Cu $\approx 90^\circ$) configurations have been extensively studied. A far richer spectrum of properties is expected from systems with intermediate bond angles, and the search for realizations of such coupling geometries has become important.

The rather poorly studied BaCu₂Si₂O₇ is a good example of a zig-zag chain network of corner-sharing CuO₄ plaquettes (Fig. 1) with intermediate values of \angle Cu-O-Cu bond angles, 124°. The crystal structure is orthorhombic, space group *Pnma*, with the cell constants being $a = 6.862(2)$ Å, $b = 13.178(1)$ Å, and $c = 6.897(1)$ Å.⁹ The spin chains run along the c crystallographic axis. In the present paper we report magnetic susceptibility measurements and inelastic neutron scattering experiments on this material. We find it to be an excellent model of weakly-coupled quantum $S = 1/2$ chains, exhibiting a crossover from 1-D behavior at high temperatures to 3-D behavior and long-range AF (Néel) order at low temperatures. As anticipated for a system with intermediate values of bond angles, the magnetic properties are extremely sensitive to slight modifications in atomic positions. This is demonstrated by preliminary susceptibility results for BaCu₂Ge₂O₇, which, unlike the isomorphous BaCu₂Si₂O₇, orders in a weak-ferromagnetic structure with a small net magnetization.

II. EXPERIMENTAL

Polycrystalline samples of BaCu₂Si₂O₇ (or BaCu₂Ge₂O₇) were prepared by conventional solid-state reaction method, using BaCO₃, SiO₂ (or GeO₂), and CuO as starting materials. The polycrystalline rods were crushed to fine powder for neutron powder diffraction studies. Single crystals were grown using the floating-zone technique from a sintered polycrystalline rod. In inelastic neutron scattering experiments we utilized an as-grown single-crystal rod (5 mm diameter \times 10 mm long). A small fragment cut to a 3 mm³ cube was used in single-crystal susceptibility measurement.

All magnetic susceptibility experiments were done with a commercial SQUID magnetometer (χ -MAG7, Conductus, Co. Ltd.) in the temperature range of 2 to 300 K. Neutron powder diffraction experiments were carried out at the

400 cells CRG diffractometer D1B at Institut Laue Langevin (Grenoble, France). Single-crystal neutron scattering studies were performed with the ISSP-PONTA triple-axis spectrometer installed at 5G beam hole of the Japan Research Reactor 3M at the Japan Atomic Energy Research Institute (Tokai, Japan). Pyrolytic graphite PG(002) reflections were used in the monochromator and analyzer. The collimation setup was 60° - 80° - 40° - 80° , with a PG filter positioned after the sample. The final neutron energy was fixed at $E_f = 14.7$ meV. The sample was mounted in a standard “ILL Orange” cryostat with the $(0, k, l)$ reciprocal-space plane in the scattering plane of the spectrometer, and the data were collected in the temperature range 2 - 15 K.

III. RESULTS

A. Magnetic susceptibility

The temperature dependences of DC magnetic susceptibility measured under $H = 10$ kOe in $\text{BaCu}_2\text{Si}_2\text{O}_7$ and $\text{BaCu}_2\text{Ge}_2\text{O}_7$ are shown in Fig. 2(a). The experimental curve for $\text{BaCu}_2\text{Si}_2\text{O}_7$ shows a sharp peak around 9 K and a broad maximum around 150 K. The $\text{BaCu}_2\text{Si}_2\text{O}_7$ data were fitted to the theoretical Bonner-Fisher (BF) curve for a one-dimensional $S = 1/2$ quantum antiferromagnet¹⁰ (solid lines). A Heisenberg exchange constant $J \approx 280$ K (24.1 meV) was obtained from this analysis.¹¹ Note that the BF fit becomes rather poor in the low-temperature region, suggesting the onset of 3-dimensional spin correlations in this regime.

To identify the low-temperature ordered structure of $\text{BaCu}_2\text{Si}_2\text{O}_7$ below 9.2 K, the anisotropy of magnetic susceptibility was studied in a single-crystal sample. The measured temperature dependences are shown in Fig. 2(b). Signs of long-range Néel ordering are clearly seen. Below 9.2 K a substantial drop is observed in χ_c , while both χ_a and χ_b change little from 9.2 K down to 2 K. This clearly points to the presence of antiferromagnetic long-range order below $T_N = 9.2$ K with crystallographic c axis being the magnetic easy axis of the system. Note that at $T \rightarrow 0$ χ_c retains a substantial non-zero value, suggesting a reduction of ordered moment, presumably due to the 1-D nature of the system. As expected, the one-dimensional character of paramagnetic phase is observed in single crystals as well. The susceptibility shows broad maxima around 180 K along all the three crystallographic directions. Fitting these data to a BF curve, and assuming an anisotropic g -factor, we obtain $g_a = 2.5$ and $g_b = g_c = 2.2$.

For $\text{BaCu}_2\text{Ge}_2\text{O}_7$ a BF analysis (dashed line in Fig. 2(a)) of the high- T part of the experimental $\chi(T)$ curve yields $J \approx 540$ K (46.5 meV), i.e., much larger than for $\text{BaCu}_2\text{Si}_2\text{O}_7$. In the low-temperature region the magnetic susceptibilities of the two isomorphous compounds become qualitatively different. The drastic increase of magnetization in $\text{BaCu}_2\text{Ge}_2\text{O}_7$ observed below 8.5 K is attributed to the appearance of uniform spontaneous magnetization. This increase is particularly well seen in the low-field measurement (Fig. 2(a), inset). The saturation value of magnetization ($\approx 6 \times 10^{-2}$ emu/g) is orders of magnitude less than 22.15 emu/g, that one would obtain if all the Cu^{2+} spins were aligned ferromagnetically. The clear dominance of c -axis antiferromagnetism in the paramagnetic phase of $\text{BaCu}_2\text{Ge}_2\text{O}_7$ suggests that the spontaneous uniform moment below 8.5 K is a result of a canted weak-ferromagnetic spin arrangement.

B. Neutron diffraction.

As a first step towards determining the magnetic structure of $\text{BaCu}_2\text{Si}_2\text{O}_7$ we performed neutron powder diffraction experiments at 2 K and 15 K, i.e., above and below the Néel temperature. Subtraction of the powder scan data collected at these two temperatures did not reveal any sign of magnetic Bragg reflections. This failure to observe any magnetic signal in the powder experiment can be attributed to a small value of ordered moment and the fact that all magnetic reflections appear on top of strong nuclear peaks (see below), not surprising for a structure with 8 magnetic Cu^{2+} ions per unit cell, and are thus very difficult to detect.

Even in the subsequent single-crystal experiment, only limited information on the magnetic structure of AF phase of $\text{BaCu}_2\text{Si}_2\text{O}_7$ could be obtained. Only one magnetic reflection, namely (011), could be reliably measured at low temperatures. The (011) *nuclear* reflection is allowed by crystal symmetry, but its intensity is fortunately relatively weak. The inset (a) in Fig. 3 shows rocking curves of the (011) Bragg peak measured above (open circles) and below (solid circles) the magnetic transition temperature. The difference between these two scans is shown in the inset (b) of Fig. 3. The measured peak intensity is plotted against temperature in the main panel of Fig. 3. The observed increase upon cooling through $T_N = 9.2$ K is attributed to long-range magnetic ordering. Intensities of several other Bragg peaks, including (031), (013), (051), (071), (053), and (035) were also measured as functions of temperature. However, the nuclear contribution to these reflections is much larger than that for (011), and no intensity increase could be observed beyond the experimental error bars upon cooling through T_N .

C. Inelastic scattering

Inelastic neutron scattering studies of spin excitations in $\text{BaCu}_2\text{Si}_2\text{O}_7$ were also performed. The rather steep spin wave dispersion along the chain axis was measured in two constant- E scans near the 1-D AF zone-center $\vec{Q} = (0, -1.5, l)$, at energy transfers $\hbar\omega = 10$ meV (Fig. 4(a)) and $\vec{Q} = (0, 0, l)$ at $\hbar\omega = 5$ meV (Fig. 4(b)). Both data sets were collected at $T = 2$ K, and transverse wave vector k was chosen to optimize focusing conditions. Even in the 10 meV scan the two spin wave branches are barely resolved. Unfortunately, for higher energy transfers the magnetic signal was too weak to be measured in the present experiment.

The spin wave dispersion along the b axis was measured at $T = 2$ K in constant- Q scans at three reciprocal-space points at the bottom of longitudinal dispersion (Fig. 5): $\vec{Q} = (0, 0, 1)$, $\vec{Q} = (0, 0.5, 1)$, and $\vec{Q} = (0, 1.1, 1)$. Clearly the transverse bandwidth (≈ 1 meV) is very small compared to that along the chain axis, which confirms the 1-D character of spin correlations in $\text{BaCu}_2\text{Si}_2\text{O}_7$. Even in the vicinity of the 3-D magnetic zone-center (011) the excitation energy appears to extrapolate to a non-zero value, i.e., the spectrum has a gap $\Delta_{(011)} \approx 1.5$ meV.

IV. DISCUSSION

All our experimental results point to that both $\text{BaCu}_2\text{Si}_2\text{O}_7$ and $\text{BaCu}_2\text{Ge}_2\text{O}_7$ should be considered as quasi-1D systems, dominated by strong intrachain antiferromagnetic exchange interactions. Long-range ordering at low temperatures occurs owing to a much weaker interchain coupling. The subtleties of the low-temperature magnetic structures and magnetic anisotropy, as well as the variations of the intrachain coupling constant J in the two systems are expected to be related to the details of the microscopic atomic arrangement.

A. Microscopic structure and magnetic interactions

Rather remarkable is the drastic (a factor of 2) difference in the intrachain AF exchange constants of the two isomorphous systems $\text{BaCu}_2\text{Si}_2\text{O}_7$ and $\text{BaCu}_2\text{Ge}_2\text{O}_7$. The AF spin chains in these species are formed by corner-sharing CuO_4 plaquettes, and the main contribution to AF interactions is expected to be the standard superexchange mechanism involving the shared O sites. A single chain is visualized in Fig. 6(a). Only the Cu sites and the shared oxygen sites are shown. The Cu^{2+} ions are almost perfectly lined up. However, the Cu-O-Cu bond angle is substantially smaller than 180° . The difference in J is most likely due to a difference in this crucial bonding angle: 124° in $\text{BaCu}_2\text{Si}_2\text{O}_7$ and 135° in the Ge-based system.⁹ Indeed we know that a larger bond angle is more favorable for superexchange involving oxygen.

Subtle structural differences between the two systems are also to be held responsible for the difference in the low- T behavior. In addition to single-ion anisotropy that manifests itself in the anisotropy of the g -factor and the gap in the spin wave spectrum (see discussion below), one should also consider the possibility of Dzyaloshinskii-Moriya asymmetric exchange interaction. The latter is allowed by local Cu-site symmetry in $\text{BaCu}_2\text{Si}_2\text{O}_7$ and $\text{BaCu}_2\text{Ge}_2\text{O}_7$, and may be responsible for the weak ferromagnetism of $\text{BaCu}_2\text{Ge}_2\text{O}_7$. The correlation between the microscopic structure and magnetic properties of $\text{BaCu}_2\text{Si}_2\text{O}_7$ and $\text{BaCu}_2\text{Ge}_2\text{O}_7$ is indeed a very interesting problem. However, at the present stage we do not have sufficient information required for a more detailed discussion of this subject, and suggest that further experiments, possibly using polarized neutron diffraction, should be performed to clarify the magnetic structures in the ordered state.

B. Weakly coupled quantum spin chains

Ignoring for now such subtleties as magnetic anisotropy, spin canting in the ordered state and the possibility of DM-interaction, we shall turn to discussing what makes the two new systems really valuable for our cause, namely the 1-D quantum antiferromagnetic aspect of their magnetic properties. In the following sections we shall demonstrate that the observed behavior of $\text{BaCu}_2\text{Si}_2\text{O}_7$ can be very well understood within the framework of existing theories for weakly-coupled $S = 1/2$ AF chains. Particularly useful for describing such systems are the chain-MF (Mean Field)^{12,13,14} and the corresponding chain-RPA (Random Phase Approximation) models.^{14,15} These approaches were previously shown to work extremely well for a number of well-characterized compounds (see for example Refs. 16, 17 and references therein).

1. A model Hamiltonian

Before we can apply these MF-RPA theories to our particular system, we have to construct a model spin Hamiltonian for $\text{BaCu}_2\text{Si}_2\text{O}_7$. A slight complication arises from a non-Bravais arrangement of magnetic ions in the crystal. Indeed, the fractional cell coordinates of Cu^{2+} are 1) $(0.25 - \delta_x, \delta_y, 0.75 + \delta_z)$, 2) $(0.25 + \delta_x, -\delta_y, 0.25 + \delta_z)$, 3) $(0.75 - \delta_x, 0.5 - \delta_y, 0.75 - \delta_z)$, 4) $(0.75 + \delta_x, 0.5 + \delta_y, 0.25 - \delta_z)$, 5) $(0.75 + \delta_x, -\delta_y, 0.25 - \delta_z)$, 6) $(0.75 - \delta_x, \delta_y, 0.75 - \delta_z)$, 7) $(0.25 + \delta_x, 0.5 + \delta_y, 0.25 + \delta_z)$, and 8) $(0.25 - \delta_x, 0.5 - \delta_y, 0.75 + \delta_z)$, where $\delta_x = 0.028$, $\delta_y = 0.004$, and $\delta_z = 0.044$. The shifts δ_x and δ_z present few problems, as they do not disturb the equivalence of nearest-neighbor Cu-Cu bonds along the a and c axes, respectively. δ_y , on the other hand, leads to alternating nearest-neighbor Cu-Cu distances along the b axis. At present we shall ignore this slight alternation, assuming $\delta_y \approx 0$ and postulating nearest-neighbor Cu-Cu bonds to be equivalent along the b axis as well. The simplest nearest-neighbor Heisenberg Hamiltonian can then be written as

$$\hat{H} = \sum_{m,n,p} \mathbf{S}_{m,n,p} [J_x \mathbf{S}_{m+1,n,p} + J_y \mathbf{S}_{m,n+1,p} + J_z \mathbf{S}_{m,n,p+1}] \quad (1)$$

Here m , n , and p enumerate the spins $\mathbf{S}_{m,n,p}$ along the a , b , and c axes, respectively. As $\text{BaCu}_2\text{Si}_2\text{O}_7$ is clearly a quasi 1-D antiferromagnet, $J_z > 0$ and $|J_z| \gg |J_y|, |J_x|$.

2. Reduction of ordered moment

One of the most important predictions of the chain-MF model is the relation between ordering temperature, magnitude of interchain coupling, and saturation moment at $T \rightarrow 0$. At the MF level the actual signs of magnetic interactions are not important and these properties are determined by the mean interchain coupling constant $|J_{\perp}| = (|J_x| + |J_y|)/2$. Schulz gives the relation between m_0 , T_N and $|J_{\perp}|$:¹⁴

$$|J_{\perp}| = \frac{T_N}{1.28\sqrt{\ln(5.8J/T_N)}}, \quad (2)$$

$$m_0 \approx 1.017 \sqrt{\frac{|J_{\perp}|}{J}}. \quad (3)$$

In our case of $\text{BaCu}_2\text{Si}_2\text{O}_7$ the susceptibility data ($T_N = 0.793$ meV and $J = 24.1$ meV) gives $m_0 = 0.11\mu_B$.

To test this theoretical prediction we have to determine the spin structure in the ordered state. Unfortunately, with only one measured magnetic reflection we can only speculate on this. Let us consider an approximate collinear magnetic state, with all spins strictly along (001), as suggested by $\chi(T)$ measurements. The two simplest possible AF structures (A and B) consistent with the presence of a substantial (011) magnetic peak are shown in Figs. 7(a) and (b). We can estimate the magnitude of saturation moment that would be required in structures A and B to produce a (011) magnetic peak of measured intensity. Comparing the measured magnetic intensity of (011) to that of two strong nuclear reflections (020) and (022), and making use of the known room-temperature crystal structure,⁹ for the saturated moment m_0 of Cu^{2+} we get $m_0 = 0.16\mu_B$ and $m_0 = 0.55\mu_B$ for structures A and B, respectively. A simple calculation of nuclear and magnetic structure factors indicates that a magnetic moment as large as $0.55\mu_B$ would be easily detected in a powder experiment at $(h, k, l\text{-odd})$ positions. The lack of any clear magnetic signal in our powder data suggests that of the two proposed structures only structure A can be realized in $\text{BaCu}_2\text{Si}_2\text{O}_7$. For structure A the estimated ordered moment is in rather good agreement with the predictions of Eq. (3). We shall thus use structure A as a working assumption for the spin arrangement in $\text{BaCu}_2\text{Si}_2\text{O}_7$. For the Hamiltonian (1) to stabilize this type of ground state we will have to assume the exchange interactions to be ferromagnetic along the a axis ($J_x < 0$), and antiferromagnetic along the b axis ($J_y > 0$).

3. Spin dynamics

As is well known, for an *isolated* antiferromagnetic $S = 1/2$ chain the dynamic structure factor can be described as a two-spinon excitation continuum.¹⁸ To a good approximation

$$S(q, \omega) \propto \frac{1}{\sqrt{\omega^2 - \omega_q^2}} \Theta(\omega - \omega_q), \quad (4)$$

where ω_q is the lower bound of the continuum given by

$$\hbar\omega_q = \frac{\pi}{2} J_{\parallel} |\sin(q)|, \quad (5)$$

and J_{\parallel} is intrachain coupling constant. This type of behavior has been seen experimentally in a number of systems, in particular KCuF_3 (Refs. 16, 19) and CuGeO_3 (Ref. 20). As mentioned above, spin correlations in *weakly coupled* quantum $S = 1/2$ spin chains are very well described by the chain-RPA model.^{14,15} As the system becomes ordered in three dimensions, the spectrum develops a mass gap $\Delta(\vec{Q}_{\perp})$ that depends on the transverse momentum transfer \vec{Q}_{\perp} . The bandwidth of transverse dispersion is of the order of J_{\perp} . This is in striking contrast with classical spin wave theory, where the transverse bandwidth is proportional to $\sqrt{J_{\perp} J_{\parallel}}$. The mass gap goes to zero only at the 3-D magnetic zone-centers, i.e., at the position of magnetic Bragg reflections. A sharp single-magnon mode is the lowest-energy excitation that is split off from the lower bound of the continuum. A two-magnon continuum then starts at $2\Delta(\vec{Q}_{\perp})$. The dispersion of the magnon branch is given by

$$(\hbar\omega_{\vec{Q}})^2 = \frac{\pi^2}{4} J_{\parallel}^2 \sin^2(Q_{\parallel}) + \Delta^2(\vec{Q}_{\perp}). \quad (6)$$

For the interchain coupling geometry of KCuF_3 (equal nearest-neighbor ferromagnetic interactions along the a and b axes) the expression for $\Delta(\vec{Q}_{\perp})$ has been derived in Ref. 15.

Near the bottom of 1-D dispersion the single mode approximation (SMA) works very well¹⁴ and to a good approximation the dynamic structure factor at $T = 0$ is the given by

$$S(\vec{Q}, \omega) \propto \frac{1}{\omega} \delta(\omega - \omega_{\vec{Q}}). \quad (7)$$

For $\hbar\omega \gg |J_x|, |J_y|$, on the other hand, it is more appropriate to use Eq. (4) for isolated chains.

The dynamic structure factor $S(\vec{Q}, \omega)$ for the non-Bravais spin lattice in $\text{BaCu}_2\text{Si}_2\text{O}_7$ can be expressed through the dynamic structure factor $S_0(\vec{Q}, \omega)$ of an equivalent system with the same exchange constants and a Bravais spin lattice. The latter is obtained by setting δ_x , δ_y and δ_z to zero. It is straightforward to show that:

$$\begin{aligned} S(\vec{Q}, \omega) &= \cos^2(2\pi h\delta_x) \cos^2(2\pi l\delta_z) S_0(\vec{Q}, \omega) \\ &+ \cos^2(2\pi h\delta_x) \sin^2(2\pi l\delta_z) S_0(\vec{Q} + \{001\}, \omega) \\ &+ \sin^2(2\pi h\delta_x) \cos^2(2\pi l\delta_z) S_0(\vec{Q} + \{100\}, \omega) \\ &+ \sin^2(2\pi h\delta_x) \sin^2(2\pi l\delta_z) S_0(\vec{Q} + \{101\}, \omega). \end{aligned} \quad (8)$$

Here we have defined $Q = (\frac{2\pi}{a}h, \frac{2\pi}{b}k, \frac{2\pi}{c}l)$. In our particular case $\delta_x, \delta_z \ll 1$, so, for not too large momentum transfers $S(\vec{Q}, \omega) \approx S_0(\vec{Q}, \omega)$. In other words, we can safely analyze the measured inelastic scans assuming an idealized Bravais arrangement of Cu^{2+} sites.

We can now rewrite Eqs. (4) and (5) to match the notation introduced above for $\text{BaCu}_2\text{Si}_2\text{O}_7$:

$$S(\vec{Q}, \omega) \propto \frac{1}{\sqrt{\omega^2 - \omega_{Q_{\parallel}}^2}} \Theta(\omega - \omega_{Q_{\parallel}}), \quad (9)$$

$$\hbar\omega_{Q_{\parallel}} = \frac{\pi}{2} J_z |\sin(\pi l)|. \quad (10)$$

The result for transverse dispersion $\Delta(\vec{Q}_{\perp})$ derived for the case of KCuF_3 by Essler *et al.*¹⁵ can also be easily adapted for use with the coupling geometry in $\text{BaCu}_2\text{Si}_2\text{O}_7$:

$$(\hbar\omega_{\vec{Q}})^2 = \frac{\pi^2}{4} J_z^2 \sin^2(\pi l) + A^2 \frac{J_y - J_x}{4} [J_y - J_x + J_x \cos(\pi h) + J_y \cos(\pi k)] + D^2. \quad (11)$$

In this formula we introduced an empirical anisotropy gap D . The dimensionless mass gap A is given by $A \approx 6.175$.¹⁴

4. Analysis of inelastic data

The dynamic structure factor, Eq. (9), convoluted with the 4-dimensional spectrometer resolution function was used to analyze the two measured constant- E scans. Reasonably good fits to the data (solid lines in Fig. 4) were obtained with only three adjustable parameters, namely J_z , an intensity prefactor, and a flat background for each scan. The refined value $J_z = 19.84$ meV is in agreement with the previous estimation, 24.1 meV, based on the experimental $\chi(T)$ curve.

For analyzing the b -axis dispersion we used the SMA given by Eq. (7), also convoluted with the resolution function. As we do not have any data for the dispersion along the a axis, to reduce the number of parameters we have assumed $|J_x| = |J_y| = J_{\perp}$. The relevant adjustable parameters for the fit were thus J_{\perp} , the anisotropy constant D , responsible for the gap at (011), and an intensity prefactor. The fitting procedure gives $J_{\perp} = 0.29(2)$ meV and $D = 1.59(4)$ meV. The resulting simulated scans are shown in solid lines in Fig. 4. On the other hand, J_{\perp} is estimated from the susceptibility data using Eq. (2),¹⁴ which gives $J_{\perp} = 0.27$ meV for $\text{BaCu}_2\text{Si}_2\text{O}_7$, in excellent agreement with what we find from the analysis of transverse dispersion.

V. CONCLUDING REMARKS

The purpose of this paper was to introduce $\text{BaCu}_2\text{Si}_2\text{O}_7$ as a new model $S = 1/2$ quantum antiferromagnet. The particular combination of intrachain and transverse coupling constants make future neutron scattering studies of this material particularly promising. Indeed, $\text{BaCu}_2\text{Si}_2\text{O}_7$ is a *better* 1-D compound than KCuF_3 with a smaller ratio of T_N / J_{\parallel} . At the same time the interchain interactions in the new silicate are sufficiently strong to make the mass gap easily observable with inelastic neutron scattering techniques. The use of cold neutrons should enable an experimental study of the double gap, i.e., the separation between the magnon branch and the 2-particle continuum. This effect in $\text{BaCu}_2\text{Si}_2\text{O}_7$ is expected to be similar to the double gap found in the dimerized state of CuGeO_3 ,²¹ but is caused by interchain interactions, rather than dimerization within the chains.

When this work was in progress we became aware of the similar susceptibility data of polycrystalline samples of $\text{BaCu}_2\text{Si}_2\text{O}_7$ and $\text{BaCu}_2\text{Ge}_2\text{O}_7$.²² These results are consistent with our data.

ACKNOWLEDGMENTS

We would like to thank T. Masuda, T. Yamada, and Z. Hiroi for valuable discussions. We also thank K. Nakajima, and T. Yoshihama for technical assistance of neutron experiments. This work is supported in part by the U.S. - Japan Cooperative Program on Neutron Scattering, the Grant-in-Aid for Scientific Research on Priority Area “Mott transition”, Grant-in-Aid for COE Research “SCP coupled systems”, and Grant-in-Aid for Scientific Research (A) of the Ministry of Education, Science, Sports, and Culture. Work at Brookhaven National Laboratory was carried out under Contract No. DE-AC02-76CH00016, Division of Material Science, U.S. Department of Energy.

* Present address: Central Research Laboratory, Hitachi Ltd.

¹ M. Hase, I. Terasaki, and K. Uchinokura, Phys. Rev. Lett. **70**, 3651 (1993).

² Y. Sasago, M. Hase, K. Uchinokura, M. Tokunaga, and N. Miura, Phys. Rev. B **52**, 3533 (1995).

³ A. Zheludev, G. Shirane, Y. Sasago, M. Hase, and K. Uchinokura, Phys. Rev. B **53**, 11642 (1996).

⁴ Y. Sasago, K. Uchinokura, A. Zheludev, and G. Shirane, Phys. Rev. B **55**, 8357 (1997).

⁵ T. Ami, M. K. Crawford, R. L. Harlow, Z. R. Wang, D. C. Johnston, Q. Huang, and R. W. Erwin, Phys. Rev. B **51**, 5994 (1995).

⁶ Z. Hiroi, M. Azuma, and M. Takano, J. Solid State Chem. **95**, 230 (1991).

⁷ N. Motoyama, H. Eisaki, and S. Uchida, Phys. Rev. Lett. **76**, 3212 (1996).

⁸ Y. Mizuno, T. Tohyama, S. Maekawa, T. Osafune, N. Motoyama, H. Eisaki, and S. Uchida, Phys. Rev. B **57**, 5326 (1998).

⁹ J. A. S. Oliveira, PhD. Thesis, *Ruprecht-Karls-Universität Heidelberg*, (1993).

¹⁰ J. C. Bonner and M. E. Fisher, Phys. Rev. **135**, A640 (1964).

¹¹ To avoid confusion, throughout the paper we will be using the notation for J in which the 1-D Hamiltonian is written as $\hat{H} = J \sum_i \mathbf{S}_i \cdot \mathbf{S}_{i+1}$.

¹² D. J. Scalapino, Y. Imry, and P. Pincus, Phys. Rev. B **11**, 2042 (1975).
¹³ I. Affleck, M. P. Gelfand and R. R. P. Singh, J. Phys. A **27**, 7313 (1994); Erratum **28**, 1787 (1995).
¹⁴ H. J. Schulz, Phys. Rev. Lett. **77**, 2790 (1996).
¹⁵ F. H. L. Essler, A. M. Tsvelik, and G. Delfino, Phys. Rev B **56**, 11001 (1997).
¹⁶ D. A. Tennant, S. E. Nagler, D. Welz, G. Shirane, and K. Yamada, Phys. Rev. B **52**, 13381 (1995); D. A. Tennant, R. A. Cowley, S. E. Nagler, and A. M. Tsvelik, *ibid.*, 13368-13380 (1995).
¹⁷ K. M. Kojima, Y. Fudamoto, M. Larkin, G. M. Luke, J. Merrin, B. Nachumi, Y. J. Uemura, N. Motoyama, H. Eisaki, S. Uchida, K. Yamada, Y. Endoh, S. Hosoya, B. J. Sternlieb, and G. Shirane, Phys. Rev. Lett. **78**, 1787 (1997).
¹⁸ G. Müller, H. Thomas, H. Beck, and J. C. Bonner, Phys. Rev. B **24**, 1429 (1981).
¹⁹ S. E. Nagler, D. A. Tennant, R. A. Cowley, T. G. Perring, and S. K. Satija, Phys. Rev. B **44**, 12361 (1991).
²⁰ M. Arai, M. Fujita, M. Motokawa, J. Akimitsu, and S. M. Bennington, Phys. Rev. Lett. **77**, 3649 (1996).
²¹ M. Ain, J. E. Lorenzo, L. P. Regnault, G. Dhaleine, A. Revcolevschi, B. Hennion, and Th. Jolicoeur, Phys. Rev. Lett. **78**, 1560 (1997).
²² T. Yamada and Z. Hiroi, private communication.

FIG. 1. A schematic view of the crystal structure of $\text{BaCu}_2\text{Si}_2\text{O}_7$. Chains of corner-sharing CuO_4 plaquettes run along the c crystallographic axis and are supported by a network of SiO_4 tetrahedra.

FIG. 2. (a) Magnetic susceptibility of polycrystalline samples of $\text{BaCu}_2\text{Ge}_2\text{O}_7$ and $\text{BaCu}_2\text{Si}_2\text{O}_7$ measured at $H = 10$ kOe. Solid and dotted lines are fits to the theoretical Bonner-Fisher curve. The inset shows an evolution of magnetization in $\text{BaCu}_2\text{Ge}_2\text{O}_7$, measured in a weak magnetic field of 100 Oe. (b) Magnetic susceptibility of single-crystal $\text{BaCu}_2\text{Si}_2\text{O}_7$ measured in $H = 1$ kOe magnetic field applied along the principal axes. Solid and dotted lines are as in (a). The inset shows magnified curves around T_N .

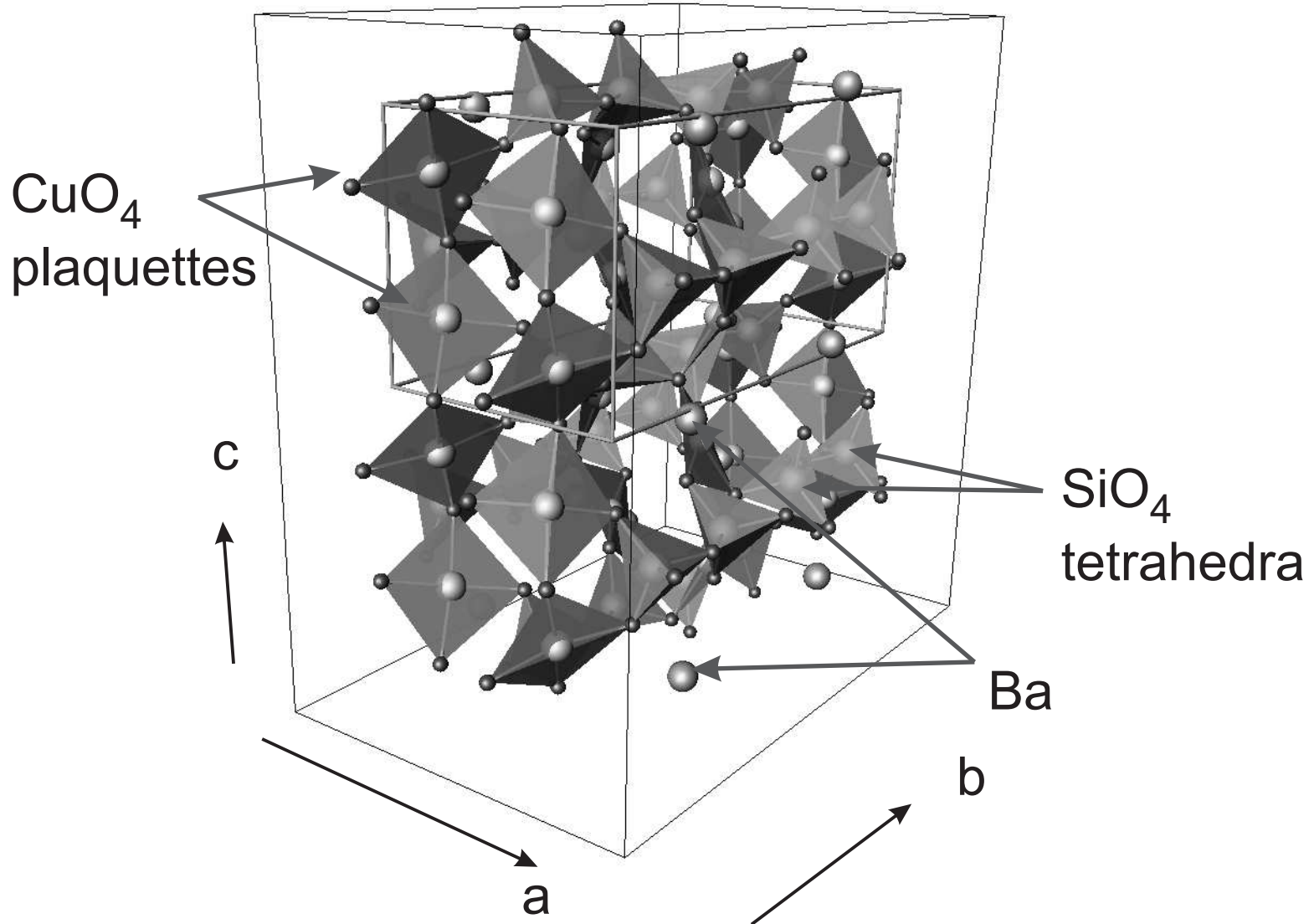
FIG. 3. Inset: (a) Elastic $\theta - 2\theta$ neutron scans through the (011) Bragg reflection collected above and below the magnetic ordering temperature in $\text{BaCu}_2\text{Si}_2\text{O}_7$. (b) The corresponding magnetic contribution obtained by subtracting the data shown in (a). Main panel: measured temperature dependence of the (011) peak intensity. Below $T_N = 9.2$ K the magnetic Bragg peak emerges on top of the (011) nuclear reflection.

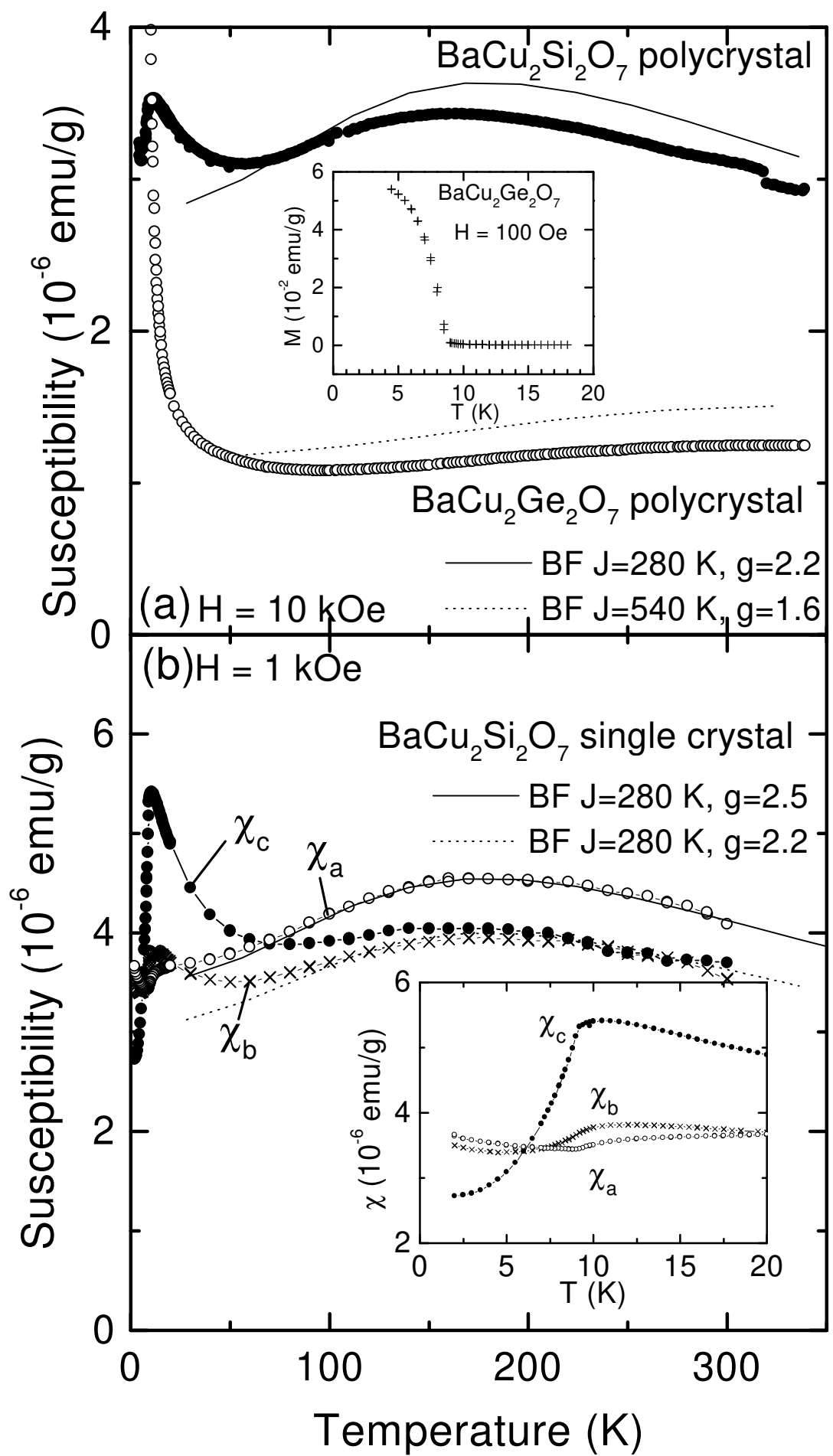
FIG. 4. Constant-energy scan along the $(0, 1.5, l)$ direction measured at $T = 2$ K in $\text{BaCu}_2\text{Si}_2\text{O}_7$, for energy transfers (a) $\hbar\omega = 10$ meV, and (b) $\hbar\omega = 5$ meV. Solid lines are theoretical fits as described in the text.

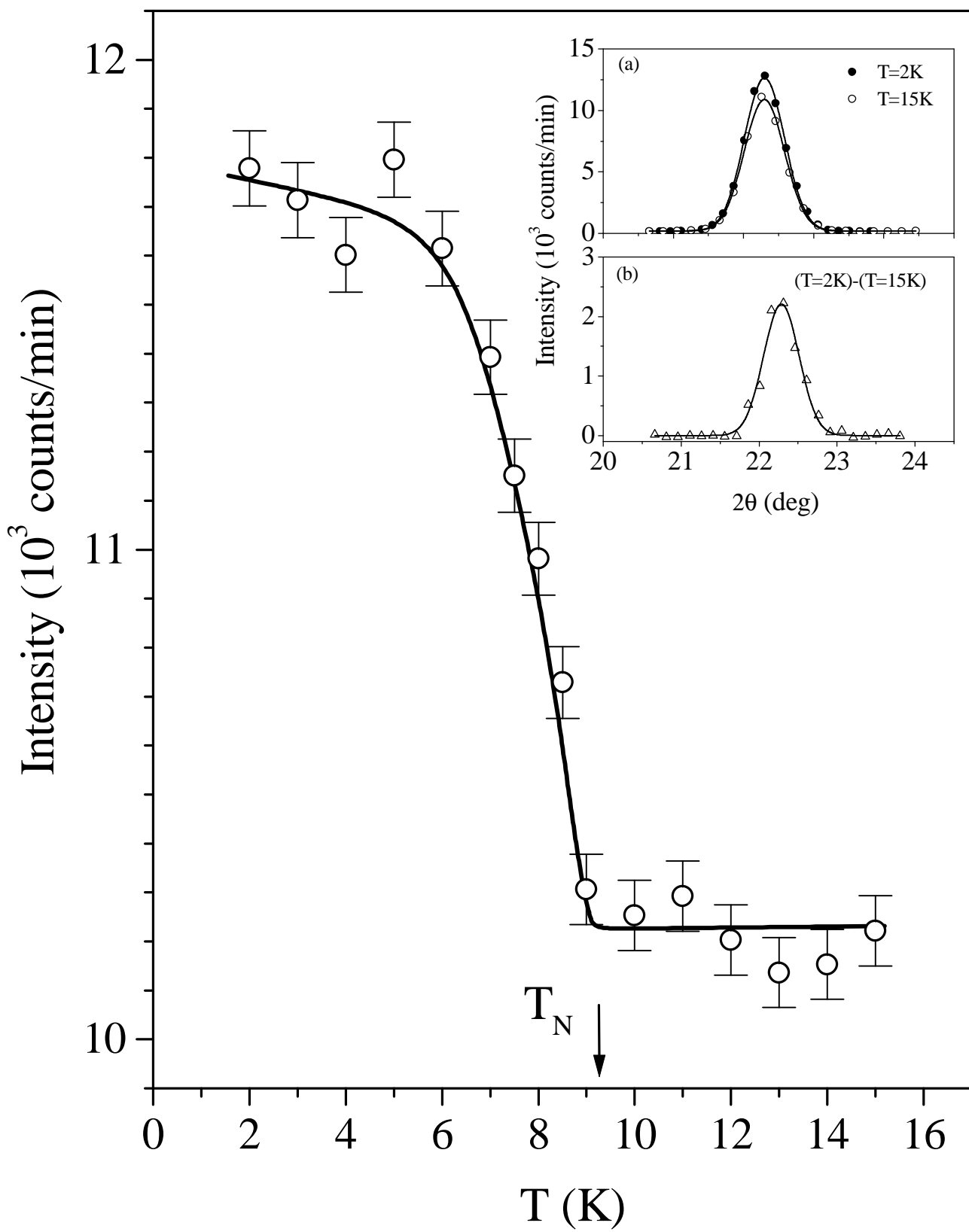
FIG. 5. Constant- Q scans measured in $\text{BaCu}_2\text{Si}_2\text{O}_7$ at $T = 2$ K. (a) $\mathbf{Q} = (0, 0, 1)$, (b) $\mathbf{Q} = (0, 0.5, 1)$, and (c) $\mathbf{Q} = (0, 1.1, 1)$. Solid lines are single-mode approximation fits, as described in the text.

FIG. 6. A schematic representation of the magnetic ion arrangement in $\text{BaCu}_2\text{Si}_2\text{O}_7$. (a) A single Cu-O chain. Cu-O-Cu bond angles are shown explicitly. (b) Relative arrangement of individual chains, projected onto the (ab) crystallographic plane. Interchain interactions are characterized by two nearest-neighbor exchange constants J_x and J_y .

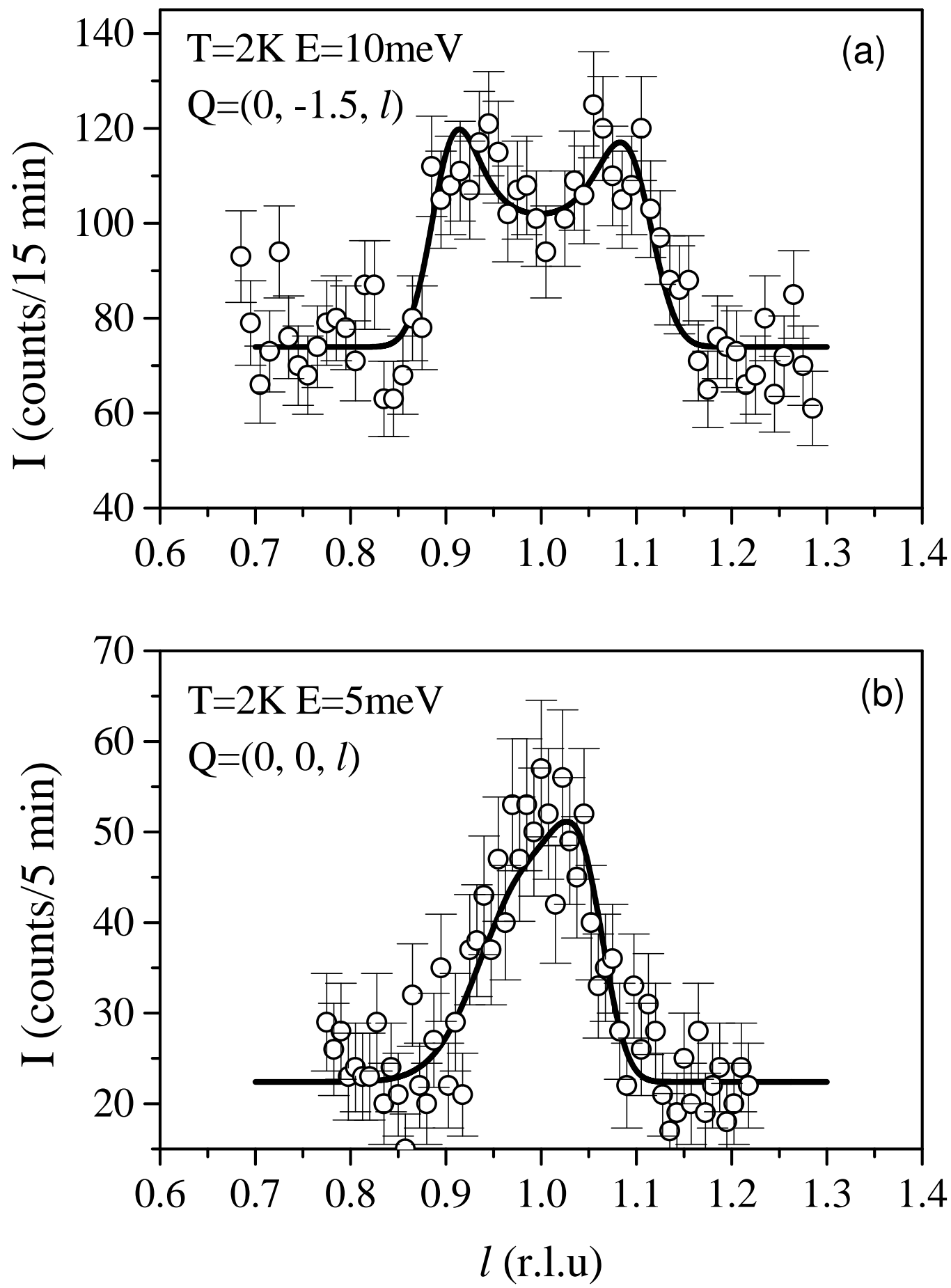
FIG. 7. Two simple collinear magnetic structures consistent with the available data on $\text{BaCu}_2\text{Si}_2\text{O}_7$, with ferromagnetic (A) and antiferromagnetic (B) nearest-neighbor coupling along the a -axis.

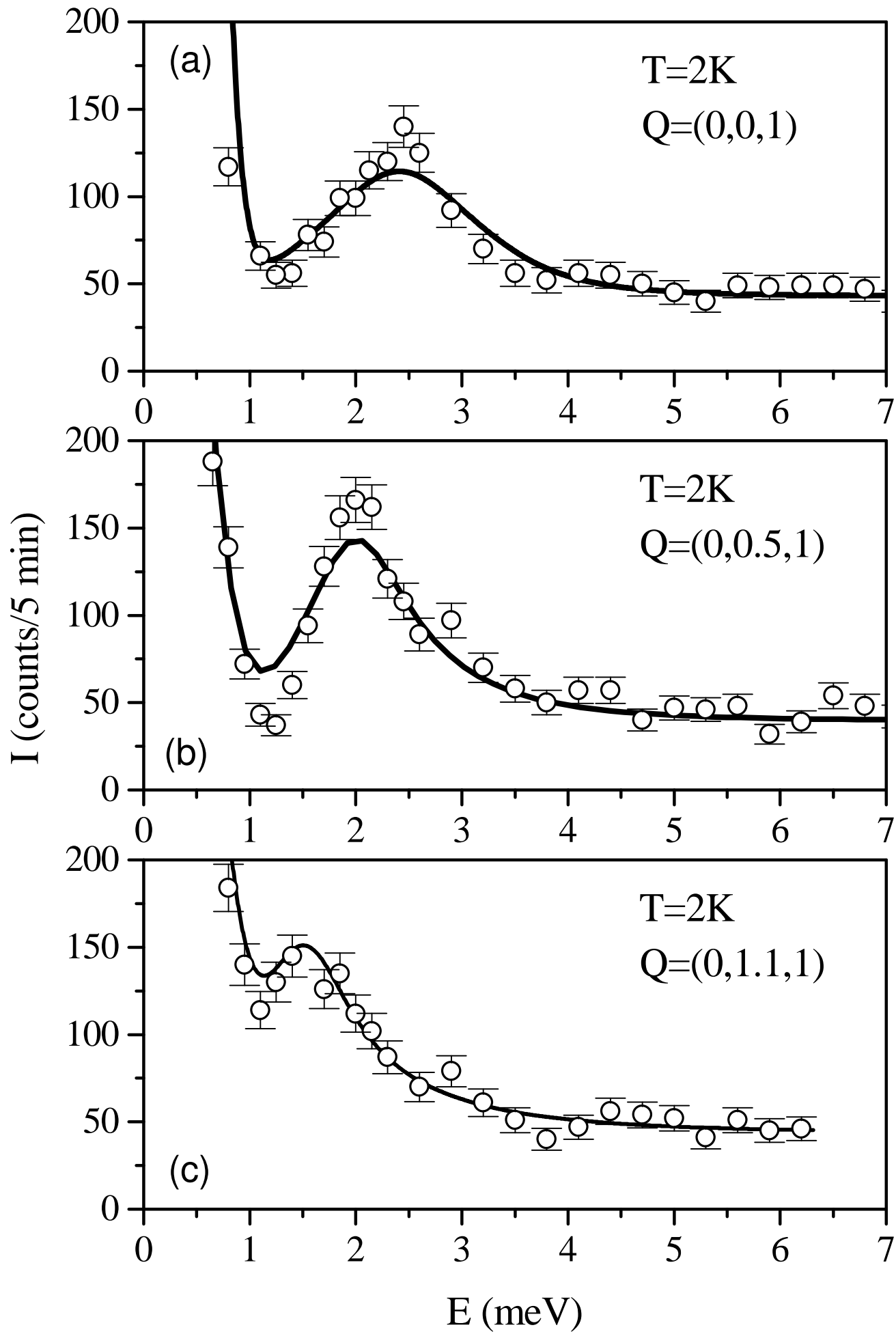


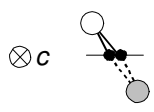
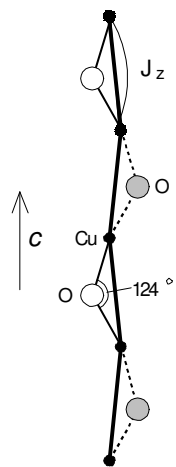




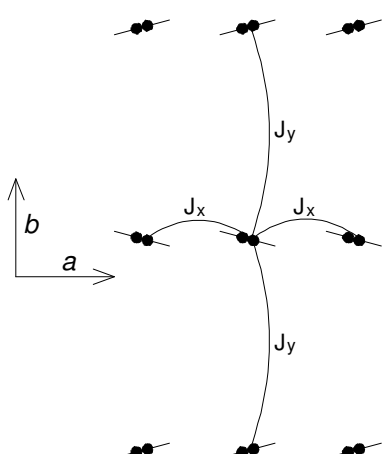
Tsukada et al., Fig. 3



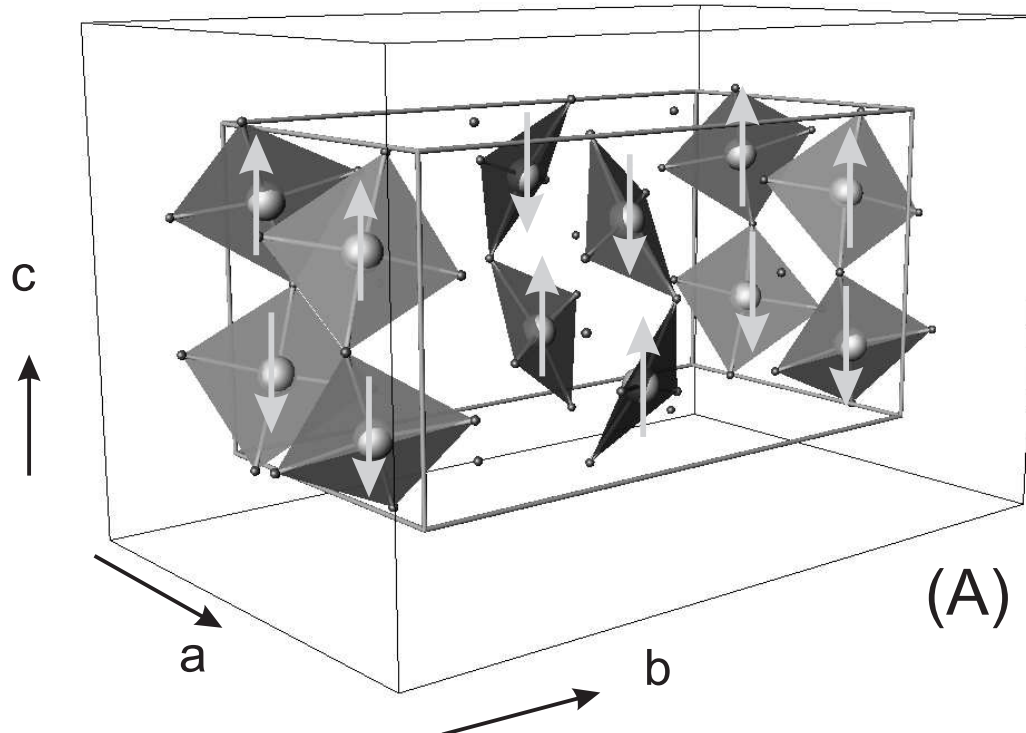




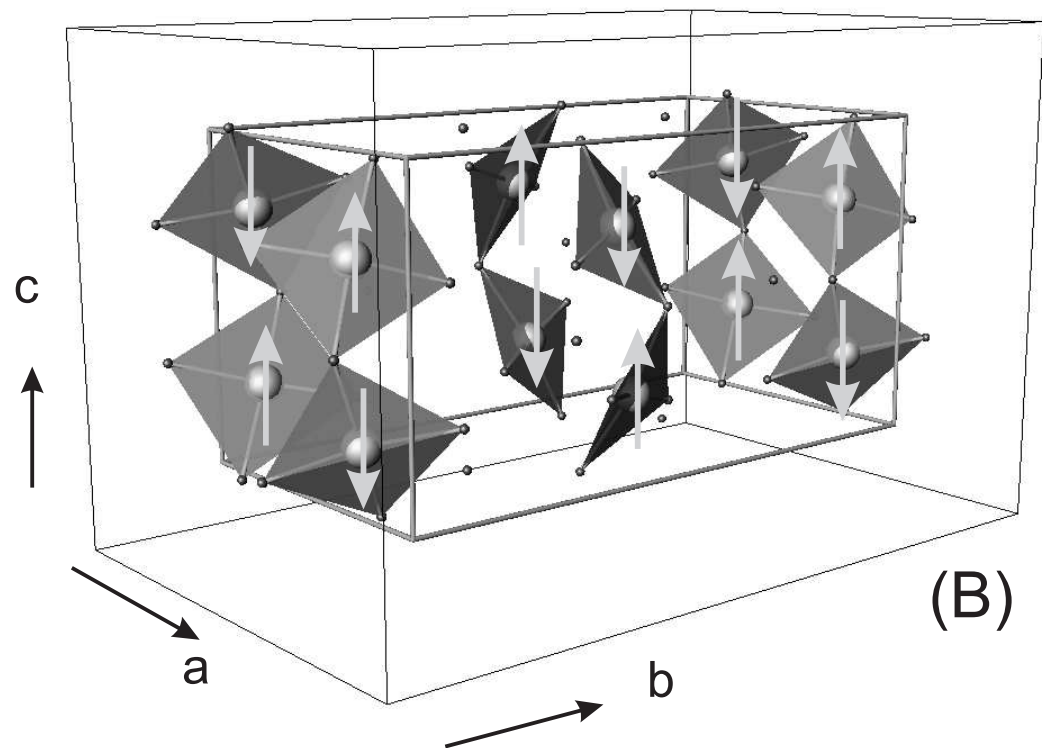
(a)



(b)



(A)



(B)